FEDSM-ICNMM2010-' 0) +(

FORMATION OF SAND RIPPLES UNDER TURBULENT FLOW SIMULATED BY LES

Yan Cui
Ritsumeikan University
gr041084@ed.ritsumei.ac.jp
Kusatsu, Shiga, Japan

John C. Wells
Ritsumeikan University
Kusatsu, Shiga,Japan

Y Quoc Nguyen
Ho Chi Minh City University
of Technology
Ho Chi Minh City, Vietnam

ABSTRACT

To simulate the initial formation of sedimentary bedforms, constrained to be in hydraulically smooth turbulent flows under bedload conditions, a numerical model based on Large Eddy Simulation (LES) in a doubly periodic domain has been developed. The numerical model comprises three parts. Given the instantaneous bed geometry, the bed shear stress distribution is obtained from a Large-Eddy-Simulation (LES) method coupled with an Immersed-Boundary-Method (IBM). Flux is estimated by the van Rijn's formula [1]. Finally, evolution of the bed surface is described by the Exner equation. "Two-dimensional bed" [2] and "three-dimensional bed" models employ, respectively, transversely averaged bed shear stress and instantaneous local shear stress to estimate the bedload flux. Based on this model, the evolution of an initial sand wave has been successfully computed. Compared to the "two-dimensional"[2] model, the three-dimensional model leads to a slightly slower propagation and a smaller sand wave. The tendency of the sand wave evolution in three-dimensional model is two-dimensional during the simulated interval.

INTRODUCTION

Subaqueous sand wave evolution is a common process, but there is still little understanding on the physics of this problem. Also there are important practical motivations for researchers to pursue this topic:
- The presence of sand waves in river beds increases the flow resistance, which in turn changes flow fluxes and water levels.
- Knowledge of sand wave sizes and propagation may help to estimate the rates of "bed load" transport of sediment.

When the Froude number is subcritical, both "ripple" and "dune" are observed. These sand waves have a similar shape, i.e. a gentle gradually varying upstream slope and an abrupt downstream, but are distinguished from each other by their relation to the flow characteristics. Ripples are considerably smaller than dunes, and their size is essentially independent of the flow depth while dune height is strongly dependent on the depth of the flow [3].

The transport of sediment particles by a flow can be in the form of bed-load and suspended load, depending on the size of the bed material particles and the flow conditions [1]. Bedload is "the part of the total load which has more or less continuous contact with the bed." Suspended load is "the part of the total load which is moving without continuous contact with the bed as the result of the agitation of the fluid turbulence."[5]

A conventional model for studying of bedload transport on a sediment bed includes a model to solve the flow field and thence the stress distribution on the bed surface, a model to transport the sediment along the bed, and a model to describe the evolution of the bed elevation according to the transport of the sediment.[6]

The most difficult part seems to be how to solve the flow field, as one has to balance between the accuracy of the solution and the cost and complexity of the model. Among available methods which explicitly represent the turbulence, hence which can satisfy the above requirements, DNS (Direct Numerical Simulation), LES and RANS (Reynolds-Averaged Navier-Stokes equations) can be considered. DNS is far too costly, leaving LES and RANS as feasible candidates ([7], [8]) at present. Keylock et al [7]suggested that LES is preferable for fluvial geomorphic and sedimentological research, since most RANS models are intended for accurate representations of the mean flow field only. For example, Chang & Scotti [9] comparing LES and with a RANS k-ω model for separating flows over ripples, reported that RANS substantially under-predicted Reynolds stress and over-predicted vertical velocity, while LES agreed very well with DNS and experiment.

In this paper our attention is mainly focused on the initial evolution of subaqueous sedimentary ripples, based on computing a highly reliable simulation of the turbulent flow field. The numerical model has three parts: 1) bed shear stress distribution obtained from flow solution by a Large-Eddy-Simulation (LES) method coupled with an Immersed-Boundary-Method (IBM), 2) bedload flux estimated by the van Rijn's formula [1], 3) evolution of the bed surface according to the Exner equation. Our "two-dimensional bed" and "three-dimensional bed" models employ, respectively, transversely averaged bed shear stress [2] and instantaneous local shear stress to estimate the bedload flux. We simulated the formation process of the first ripple under hydraulically smooth conditions (grain Reynolds number $\mathrm{Re}_p = 0.5$) in the 2D and 3D models. We found that smaller-scale "microforms" appear on the bed surface in the three-dimensional model. Results of the 2D and 3D models are compared.

NUMERICAL MODEL

To build a computational model to study the initiation and evolution of ripples, simplifying assumptions are unavoidable. The present work assumes that

- The flow is hydro-dynamically smooth (the grain Reynolds number $\text{Re}_p \leq 2.5$), i.e. roughness of the bed is neglected [3];
- Suspended sediment may be neglected, as only bedload transport is observed to dominate ripple formation [10][11][12][13];
- Time scale of flow development is much shorter than that of the bedform development [14]. Accordingly, the bed surface is treated as fixed while the flow field is solved in an interval of 100 time steps to allow the flow field to adapt to the new bed profile.

The Governing Equations of Flow.

The governing equations for LES coupled with IBM are the incompressible N-S equations, as filtered by a low-pass spatial filter. In IBM an artificial body force f is added to impose the no-slip condition of solid boundaries:

$$\frac{\partial \bar{u}_j}{\partial x_j} = 0 \tag{1a}$$

$$\frac{\partial \bar{u}_i}{\partial t} + \bar{u}_j \frac{\partial \bar{u}_i}{\partial x_j} = -\frac{1}{\rho}\frac{\partial \bar{p}}{\partial x_j} - \frac{\partial \tau_{ij}}{\partial x_j} + \nu \frac{\partial^2 \bar{u}_i}{\partial x_j \partial x_j} + f_i \tag{2a}$$

where " $\bar{\ }$ " indicates the filter operator, $\bar{u}_i$ is the filtered velocity component in i direction, i = 1, 2, 3, and $(x_1, x_2, x_3) = (x, y, z)$, ρ is the fluid density, p is the dynamic pressure, τ_{ij} is the sub-grid stress(SGS), and ν is the fluid kinematic viscosity.

The subgrid stress model is the Shear-Improved Smagorinsky model proposed by Lévêque et al. [15]:

$$\tau_{ij} - \frac{1}{3}\delta_{ij}\tau_{kk} = -2\nu_T \bar{S}_{ij} \tag{3}$$

with $\quad \bar{S}_{ij} = \frac{1}{2}\left(\frac{\partial \bar{u}_i}{\partial x_j} + \frac{\partial \bar{u}_j}{\partial x_i}\right) \quad$, $\quad \nu_T = \left(C_s \bar{\Delta}\right)^2 \left(\left|\bar{S}\right| - \left|\langle \bar{S} \rangle\right|\right)$, and

$\left|\bar{S}\right| = \left(2\bar{S}_{ij}\bar{S}_{ij}\right)^{1/2}$, where C_s=0.16 and $\bar{\Delta} = \left(\bar{\Delta}_x \bar{\Delta}_y \bar{\Delta}_z\right)^{1/3}$

$\bar{\Delta}_x$, $\bar{\Delta}_y$ and $\bar{\Delta}_z$ are the local grid spacings in the x, y, z directions, respectively. $\langle\ \rangle$ denotes "local ensemble average", which is performed in the spanwise direction for models of two-dimensional bedload, and in both spanwise direction and along time in models of three-dimensional bedload.

In IBM, the computational domain includes both the solid portions, Ω_s, and the fluid portions, Ω_f, on a fixed Cartesian grid system, and the same governing equations are applied on the whole domain; see Figure 1. The artificial body force f is added to the Navier-Stokes equation to account for the presence of the solid portions. IBM simplifies grid generation, and
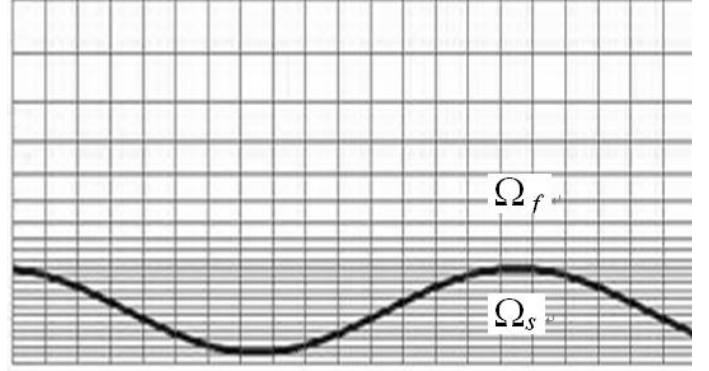

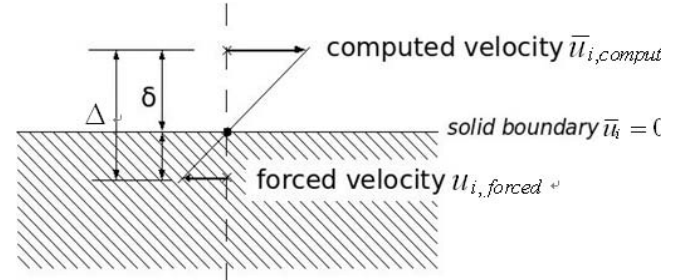Figure 1 An example of IBM grid for computing flows over a wavy bed

Figure 2 Forcing strategy in IBM

avoids regenerating the computational grid as the solid domain changes shape.

The artificial force f is used to represent the solid parts. Therefore, f should exist only on the solid portion, i.e. $f_i = 0$ in Ω_f

There are many strategies for the artificial body force f. Fadlun et al. [16] proposed a linear *velocity interpolation* method. The velocity of the point nearest to the solid surface is computed via a linear interpolation so that it satisfies $\bar{u}_i = 0$ right on the solid boundary (fixed bed). As shown in Figure 2, let Δ and δ be the grid spacing and the distance from the point outside but nearest to the solid surface, respectively; $\bar{u}_{i,computed}$ be the velocity obtained from equation (1a) and (2a) at the point outside, but nearest to the solid surface; and $u_{i,forced}$ is the imposed velocity at the point inside but nearest to the solid surface. According to Fadlun et al. [16], $u_{i,forced}$ can be computed as following:

$$u_{i,forced} = -\bar{u}_{i,computed}\frac{\Delta - \delta}{\delta} \tag{4}$$

The governing equation (1a) and (2a) are nondimensionalized by fluid density ρ, mean friction velocity $u_{\tau 0}$ and total flow depth H. Each variable in equation (1a) and (2a) is nondimensionalized as followings:

$$\tilde{t} = \frac{t}{H/u_{\tau 0}}, \quad \tilde{x}_i = \frac{x_i}{H}, \quad \tilde{\tau}_{ij} = \frac{\tau_{ij}}{u_{\tau 0}^2}, \tilde{P} = \frac{p}{\rho u_{\tau 0}^2} + \tilde{\tau}_{kk},$$
$$\tilde{f}_i = \frac{f_i H}{u_{\tau 0}}, \quad Re_\tau = \frac{u_\tau H}{\nu}.$$

where "~" indicates a nondimensionalized parameter. The governing equations become:

$$\frac{\partial \tilde{\bar{u}}_j}{\partial \tilde{x}_j} = 0 \qquad (1b)$$

$$\frac{\partial \tilde{\bar{u}}_i}{\partial \tilde{t}} + \tilde{\bar{u}}_j \frac{\partial \tilde{\bar{u}}_i}{\partial \tilde{x}_j} = -\frac{\partial \tilde{P}}{\partial \tilde{x}_i} + (\tilde{\nu}_T + \frac{1}{Re_\tau}) \frac{\partial^2 \tilde{\bar{u}}_i}{\partial \tilde{x}_j \partial \tilde{x}_j} + \tilde{f}_i \qquad (2b)$$

Boundary Conditions

Periodic boundary conditions are applied in the stream (x) and span (z) directions. No-slip conditions are applied at lower boundary and free-slip conditions on upper boundary.

The artificial force f by IBM can be replaced by an implicit boundary condition: The velocities at the points inside Ω_s but nearest to the bed surface are computed by equation (4).

Sediment Motion

In the present model, the shear velocity u_τ is computed from the shear stress, as averaged during an interval of 100 LES time steps:

$$u_\tau^2 = \nu \frac{\partial \bar{u}_\varsigma}{\partial \eta_\varsigma} \qquad (5)$$

where $\bar{u}_\varsigma$ is the time-averaged velocity component along the bed surface, and η is the surface-normal direction. In our model, we use two definitions of $\bar{u}_\varsigma$: transversely averaged velocity in two-dimensional bed model and local velocity in three-dimensional bed model.

θ_0 is the mean Shields number:

$$\theta_0 = \frac{u_{\tau 0}^2}{(s-1)gd}, \qquad (6)$$

where s is the ratio of grain density to fluid density, d is the grain diameter, and Re_p is the grain Reynolds number:

$$Re_p = \frac{u_{\tau 0} d}{\nu}, \qquad (7)$$

The local Shields number θ is:

$$\theta = \frac{u_\tau^2}{(s-1)gd} = \left(\frac{u_\tau}{u_{\tau 0}}\right)^2 \theta_0 \qquad (8)$$

There are a number of formulae for bedload transport proposed in the literature [17]. Most of them are valid only for high grain Reynolds numbers. To our knowledge, the only formula that is also valid for low grain Reynolds numbers is the equilibrium bedload flux equation by van Rijn [1]:

$$q_{eq} = 0.053 \frac{T^{2.1}}{d_*^{0.3}} \left[(s-1)g\right]^{0.5} d^{1.5} \qquad (9)$$

where $\tilde{q}_{eq}$ is the equilibrium bedload flux, and d_* is the particle mobility parameter:

$$d_* = \left[\frac{1}{\theta_0} Re_p^2\right]^{1/3} \qquad (10)$$

and T is the transport stage parameter

$$T = \frac{\theta}{\theta_c} - 1.0, \qquad (11)$$

and θ_c is the critical Shields parameter. Kovacs and Parker [18] proposed a vectorial formulation for θ_c on combined transverse and longitudinal sloping beds:

$$\left|\frac{\theta_c}{\theta_{c0}} \hat{s} + \frac{\bar{k}_t}{\tan \varphi_s}\right| = \left|\bar{k}_n\right| \qquad (12)$$

where θ_{c0} is the critical Shields number for zero-slope bed, $\hat{s}$ is the direction of shear stress, $\bar{k}_n$ (respectively, $\bar{k}_t$) is the component of the unit vertical vector normal (tangent) to the tangent plane to the bed surface. The friction angle φ_s is reported in the range of $\tan \varphi_s = [0.35\text{-}0.72]$ with an average of $\tan \varphi_s = 0.63$[14].

According to Kennedy [19] and Nakagawa & Tsujimoto [20], one of the principal causes of the bed instability is a phase lag between the sediment transport and the bed shear stress. To model this lag, or the non-equilibrium nature of sediment transport, "the rate of sediment exchange between bed and flow was assumed proportional to the difference between the actual instantaneous sediment load and the equilibrium sediment load, and related to the so called non-equilibrium adaptation length, which characterizes the distance for sediment to adjust from a non-equilibrium state to an equilibrium state" [21]. Quantifying this concept, Bui et al. [22] proposed a two-dimensional non-equilibrium bed-load transport equation:

$$\frac{\partial (\alpha \tilde{q}_b)}{\partial x} + \frac{\partial (\beta \tilde{q}_b)}{\partial z} = -\frac{\tilde{q}_b - \tilde{q}_{eq}}{\tilde{l}_{eq}} \qquad (13)$$

where $\tilde{q}_b$ is the local bedload transport rate, x is the longitudinal direction, z is the transverse direction, α, β are the direction cosines determining the components of $\tilde{q}_b$, i.e. the direction cosines of $\hat{s}$ in x and z directions, determined by equation (12); $\alpha = 1$, $\beta = 0$ in two-dimensional bedload model. $\tilde{l}_{eq}$ is the adaption length. Significant dependence of results on the adaptation length parameter has been reported[23], [24], [25]; here we adopt the adaption length taken as the average saltation step length proposed by van Rijn [1]:

$$\tilde{l}_{eq} = 3\left(\frac{d}{H}\right) d_*^{0.6} T^{0.9} \qquad (14)$$

Evolution of the bed surface is described by the Exner equation

$$(1-n)\frac{\partial \tilde{h}}{\partial \tilde{t}} = -\left(\frac{\partial (\alpha \tilde{q}_b)}{\partial x} + \frac{\partial (\beta \tilde{q}_b)}{\partial z}\right) \qquad (15)$$
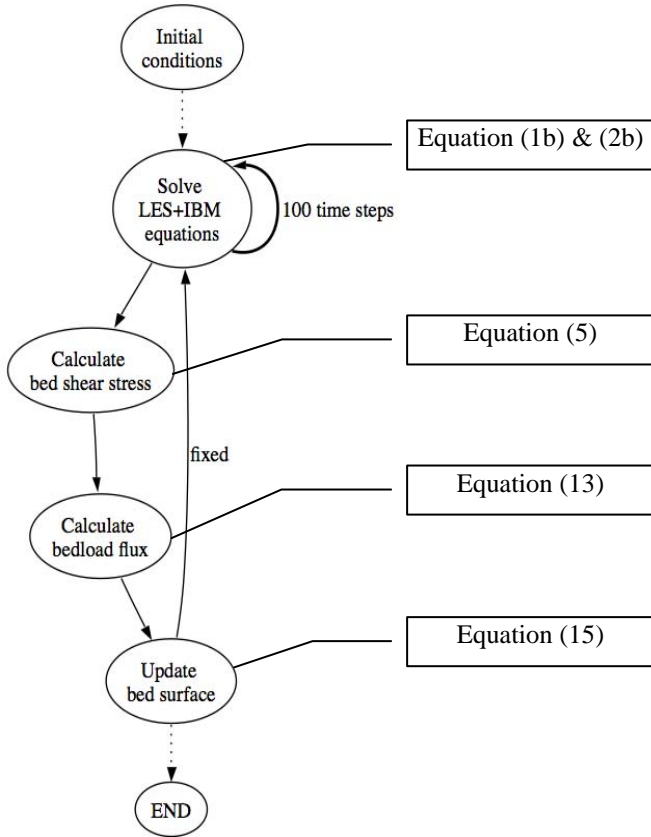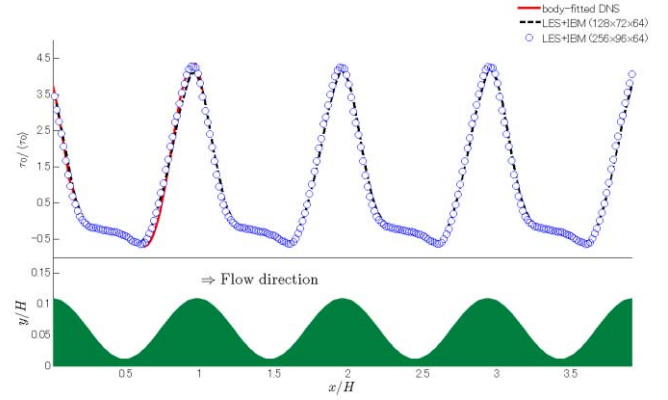
Figure 3 Computational procedure

Figure 4 Shear stress distribution over fixed sinusoidal beds, LES+ IBM, with two different grids, vs. body-fitted DNS results by De Angelis et al [27]. (Figure from Nguyen & Wells [2])

where $\tilde{h}$ is the evolution of the bed surface and n is the porosity of the bed material.

Figure 3 shows the main computational procedure of the model. The three-dimensional flow field is solved by LES coupled with IBM while the bed surface is fixed. Governing equations are solved in staggered grid with 4th order central discretization in space and 2nd-order Adams-Bashforth method for time marching [26]. After solving this hydrodynamic model over 100 time steps, the time- averaged flow field is applied to compute the bed shear stress. Then the bedload flux is estimated by van Rijn's formula [1], and the bed surface is updated by the Exner equation. We use both the two-dimensional model proposed by Nguyen & Wells [2], in which transversely averaged bed shear stress is applied to estimate the sediment flux, and the three-dimensional model according to our recent research, applying local shear stress which is non-uniform in the spanwise direction. These three steps are iterated continuously.

MODEL VALIDATION

The time-averaged bed shear stress distribution computed by the present LES+ IBM code for flows over fixed sinusoidal beds in which there is strong separation, has been compared to the body-fitted DNS results by De Angelis et al [27] for which the wave length $\Lambda = 1.04H$, $\mathrm{Re}_{\tau 0} = 170$, wave height

$\alpha = 0.5H$. The grid is ($256 \times 96 \times 64$) or ($128 \times 72 \times 64$) points in a domain of ($H_x = 4H$) $\times$ ($H_y = H$) $\times$ ($H_z = \pi H$), with $\Delta_x^+ = \Delta_z^+ \approx 30.0,$ and $\Delta_{y\,\min}^+ = 0.93$. The boundary conditions are the same in both the LES+IBM and the DNS. In the x and z directions, the flow is assumed periodic. The lower wall is no-slip, while the upper one is free-slip. The computed bed shear stress distributions are plotted in Figure 4 together with the DNS results. The LES+IBM code is tested with two different grid resolutions; good agreement can be observed. Comparing the results between the two computational methods, the agreement is seen to be excellent in this test. More details and validation of the two-dimensional model can been found in Nguyen & Wells [2].

Another test of the first wave evolution from an initial bed profile with one sinusoidal half-wave in two-dimensional model has been studied [2]. $H^+ = 300$, and $\theta_0 = 0.55$，the grid is ($256 \times 72 \times 32$) points in a domain of ($H_x = 7.68H$) $\times$ ($H_y = H$) $\times$ ($H_z = 0.96H$) with $\Delta_x^+ = \Delta_z^+ \approx 30.0,$ and $\Delta_{y\,\min}^+ = 0.93$. The depth of sand is $0.05H$ and the height of the initial sand wave is $A = 0.002H$. The time step is $\Delta t = 1.0 \times 10^{-4}$, and it takes about 50 hours to compute a series of 2.0×10^5 time steps on a standard workstation.

In the two-dimensional model by [2], Re_p was varied in the range [0.5, 2.5]. The wave lengths of the ripples obtained at each Re_p are plotted in Figure 5, together with the experimental results by Kuru et al. [28], Coleman and Melville [11], Coleman et al. [12], and Langlois and Valance [13]. That the computed points are distributing on the lower limit of the experimental ones shows the agreement between them. Results differ since we are at present short of some factors that determine sediment transport, such as the friction angle φ_s , and the development time varies between the experiments.
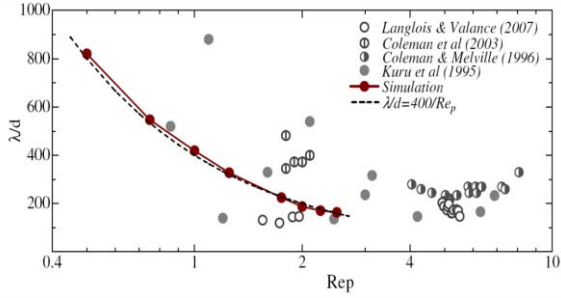
Figure 5 Length of the first sand wave developing from a flat bed: numerical [2] vs. experimental results.
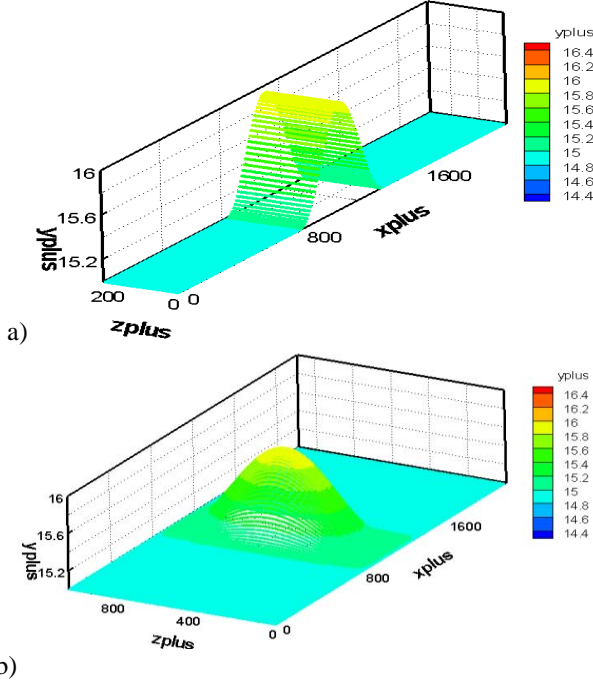

a)

b)

Figure 6 Initial bed shape for the two-dimensional model (a) and three-dimensional model (b). The height of the initial sand wave is $\Delta y^+ = 1$.

NUMERICAL RESULTS AND DISCUSSION

Figure 6(a) shows an example of the evolution from an initial bed profile of the second test above [2] when $Re_p = 0.5$. The bed profile is plotted at different nondimensionalized times, $\tilde{t} = t u_{\tau 0} / H$. From the crest of the initial wave, shown in Figure 6(a), the crest of the initial wave first grows in height, as in Figure 7. The wave crest then broadens streamwise until the downstream end of the wave starts being eroded strongly, with the scoured sediment deposited further downstream, at $\tilde{t} \simeq 5.3$ in this example. Once two troughs can be identified fore and aft of the wave, the wave is identified as "sand-wavelet".

Figure 8 is the profiles of sediment flux $\tilde{q}_b$, bed shear stress $\tau_0 / <\tau_0>$, and bed level Y^+ over the "sand-wavelet" when $\tilde{t} \simeq 6.0$, at which the first sand wavelet has appeared and begins to propagate downstream. Nguyen & Wells [2] suggested that the peaks of the friction velocity distributions are
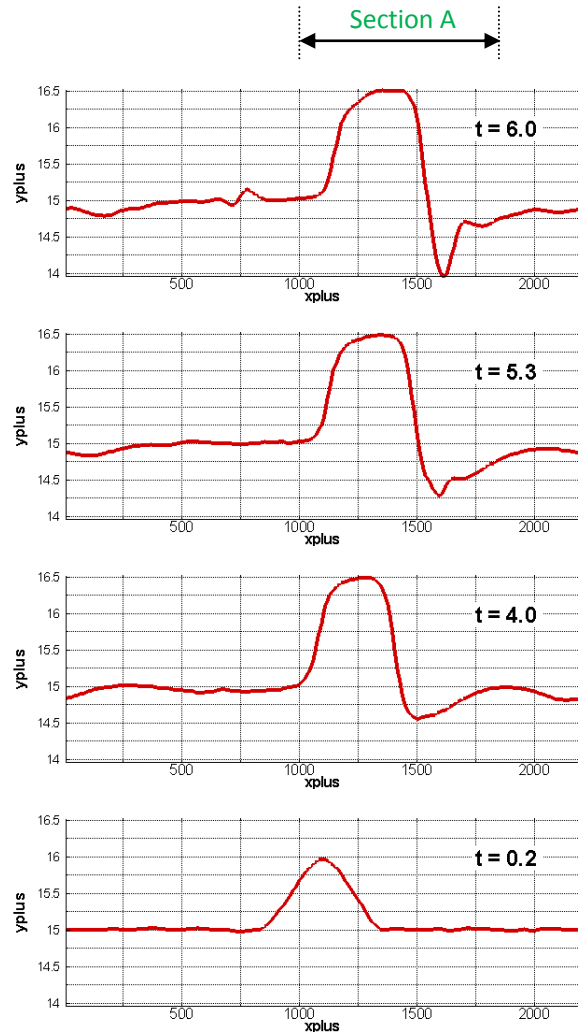

Figure 7 Profiles of the first sand wave developing at bed with an initial perturbation of one sinusoidal wave in two-dimensional model. Flow from left to right. From bottom: $\tilde{t} = 0.2, 4.0, 5.3, 6.0$. The first sand wave is identified at $\tilde{t} \simeq 5.3$.

always before the peaks of the "sand-wavelet". In Figure 8, the peaks of the curves are distinguished, but we can see the trough of the shear stress occurs before the trough of the bed surface, i.e. there is a phase lag between the two. The lag $\tilde{l}_{eq}$ between the shear stress and the sediment flux is barely distinguishable in this figure. We can also see from the figure that such a "sand-wavelet" does not cause flow separation, i.e. the shear stress is positive everywhere. The waves growth in height is also due to the phase lag between the bed shear stress and the bed profile. The peak of the bed shear stress distribution is upstream of the peak of the bed profile. After the peak of the bed shear stress, the longitudinal gradient of bed shear stress gradient turns negative, which helps the peak of the wave in bed height amplify further.
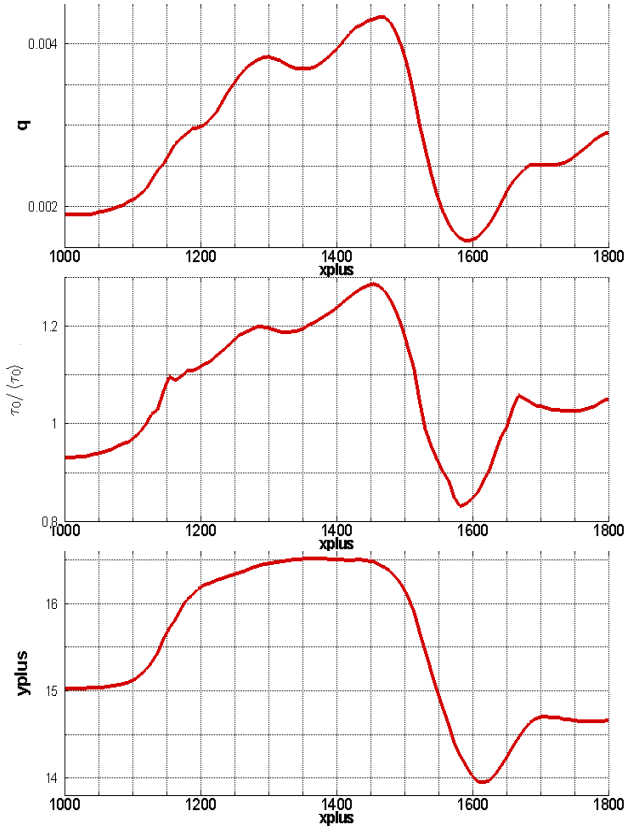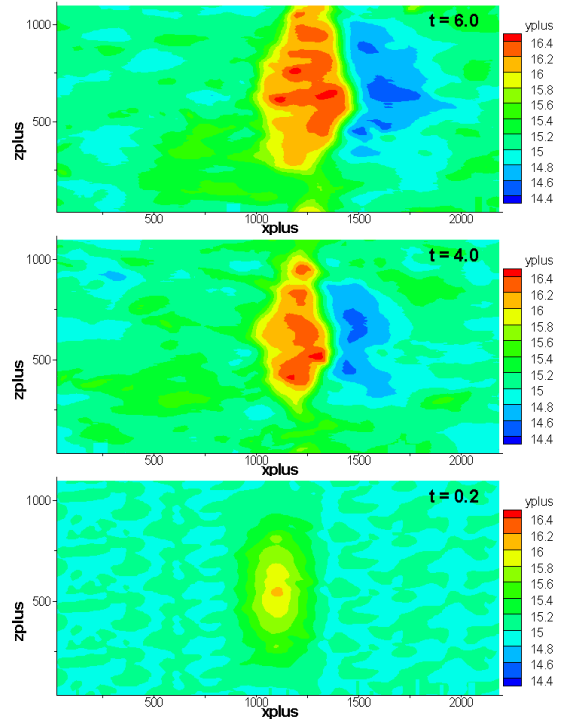
Figure 9 Three-dimensional bed planform of the first sand wave developing at the three-dimensional sand wave in Figure 6(b). From bottom: $\tilde{t} = 0.2,\ 4.0,\ 6.0$.

Figure 8 Profiles of sediment flux and bed shear stress over the "sand-wavelet" when $\tilde{t} \simeq 6.0$ (Section A in Figure 7) From top to bottom: sediment flux $\tilde{q}_b$; bed shear stress $\tau_0 / <\tau_0>$, bed level Y^+.

A three-dimensional bedload model has also been applied to compute the sediment transport. Again, we employ a fully 3D turbulent flow solver. The difference between these two models is that we use the local shear stress instead of the shear stress averaged in the z direction over the entire width, to estimate the fluxes of three-dimensional bedload transport. Also, a fourfold wider domain is adopted to weaken the periodicity constraint. With a domain of $(H_x = 7.68H) \times (H_y = H) \times (H_z = 3.84H)$, the number of grid points is about $250,000(256 \times 72 \times 128)$. And it takes about 150 hours to compute a series of 2.0×10^5 time steps.

As shown in Figure 6(b) the initial three-dimensional sand wave occupies the center of the domain, and the height of the sand wave is $\Delta y^+ = 1$. Figure 10 shows the three-dimensional bed planform of the first sand wave developing from the three-dimensional wave in Figure 6(b); we can see small three-dimensional perturbations appear on the bed surface when $\tilde{t} \approx 0.2$. Like the two-dimensional model, the sand wave grows in height at the beginning, then at $\tilde{t} \approx 4.0$ the downstream trough (the blue region) becomes deeper with the growing of the crest (the yellow-red regions. Also, by checking the

downstream ends (right side) of the trough and crest when $\tilde{t} = 6.0$, we can see the propagation of the ripple is not symmetrical in the z direction.

Continuing from Figure 9, Figure 10 shows the subsequent development of the three-dimensional bed planform at $\tilde{t} = 8.0,\ 16.0,\ 24.0$. The width of the ripple keeps growing stream-wise, but the downstream end of the trough is approximate parallel to the z direction. Any three-dimensional quality of ripple propagation becomes unclear at this stage. Figure 11 compares the instantaneous bed surfaces in the central x-y plane (blue lines), surfaces averaged in z-direction (green lines) and results from the two-dimensional model (red lines) when $\tilde{t} = 8.0,\ 16.0,\ 24.0$. As in Figure 8 the upstream face (left side) of the sand wave experiences a strong positive gradient of the bed shear stress, or equivalently of the bedload flux, leading to bed erosion according to the Equation (15). After maintaining positive gradient, the bed shear stress reaches a peak and then experiences negative gradient before returning to the average value. Due to the negative gradient of the bed shear stress, sediment is deposited. This explains the fact that the scoured sediment is deposited over the area just downstream of an existing wave to form a new wave. The more the sediment is scoured around, the deeper that trough becomes, which the stronger the gradient of the bed shear stress. Accordingly, the sand wave is continuously fed and grows gradually. The sediment is scoured over the upstream face where the gradient is positive and deposited in the lee where the
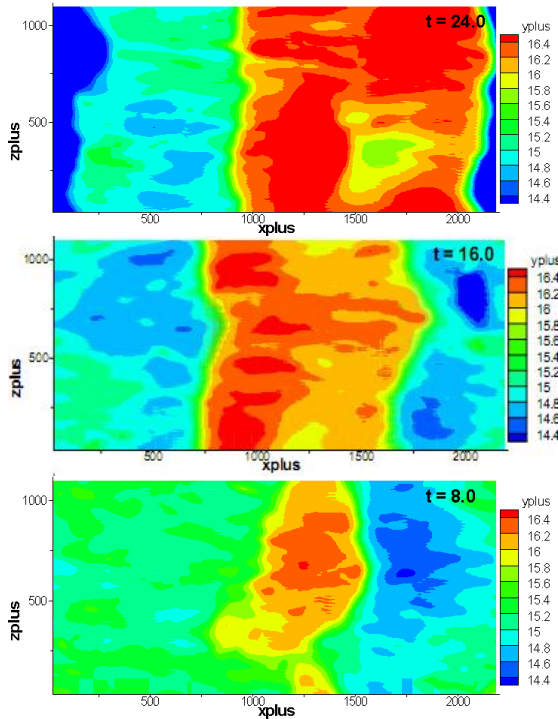
Figure 10 Three-dimensional bed planform of the sand wave propagation, From bottom: $\tilde{t} = 8.0,\ 16.0,\ 24.0$.

Figure 11 Comparison of the instantaneous bed surfaces in the center x-y plane (blue line), surfaces averaged in z-direction (green line) and results from the two-dimensional model (red line) when $\tilde{t} = 8.0,\ 16.0,\ 24.0$.
.

gradient is negative. This process makes the wave propagate downstream. Compared to the two-dimensional model, the three-dimensional model yields a slightly slower propagation and smaller sand wave during the duration simulated.

The difference between the instantaneous bed surface in the central x-y plane and the z-averaged surface reflects the non-uniform profiles in the span direction. We can see from these figures that the instantaneous bed surface in the central x-y plane and the surface averaged in the z-direction match better when $\tilde{t} = 24.0$, which means the tendency of the ripple growth is two-dimensional.

CONCLUSIONS

A numerical model has been developed to simulate the initial formation of ripples, in hydraulically smooth turbulent flows under bedload conditions. A simulation of the evolution of the initial bed profile with small perturbations has been studied. Two kinds of bed models, "two-dimensional"[2] and "three-dimensional" have been applied.

The initiation and propagation of ripples from flat beds with a half-sinusoidal wave have been simulated. The relationship of sediment evolutions and bed shear stress has been discussed and results are compared between "two-dimensional"[2] and "three-dimensional" models, and to the authors' knowledge, this is the first work ever reported on the numerical simulation of initial evolutions of three-dimensional ripples. The three-dimensional model leads to a slightly slower propagation and a smaller sand wave. But the tendency of the sand wave evolution in three-dimensional model is two-
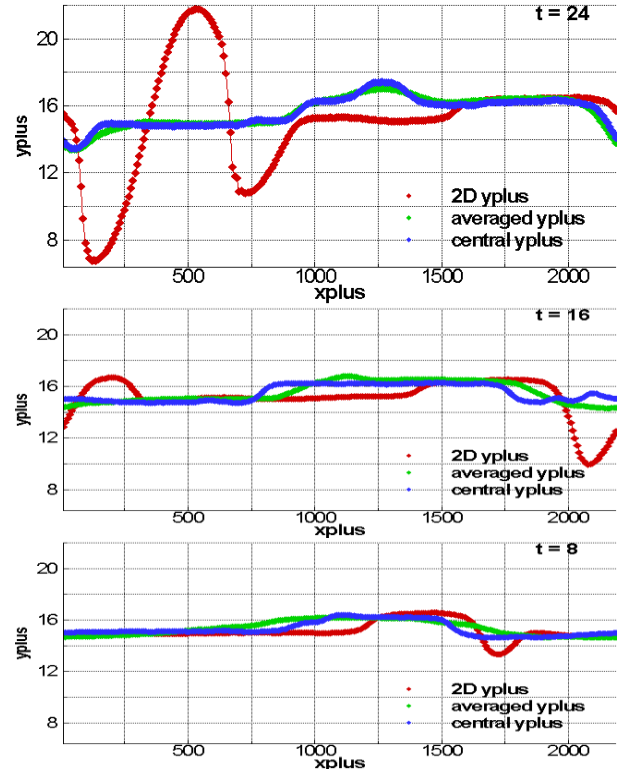
dimensional during the interval simulated So the two-dimensional model could be reasonable. Further results are still needed to check the validity of the two-dimensional model.

Up to the present, our 3D bed model has just been tested with a representative value grain Reynolds number $Re_p = 0.5$. As shown in Figure 3, $Re_p = 0.5$ is near the smallest experiment value in available literature. However, more tests with Re_p varying in the range [0.5, 2.5] are needed. Beyond that, it is important to extend the LES-IBM technique to handle transitional roughness, i.e. $Re_p > 2.5$.

REFERENCES

[1]   van Rijn L. C., 1984, "Sediment Transport, Part I: Bed Load Transport," Journal of Hydraulic Engineering, **110**(10), pp. 1431–1456.

[2]   Nguyen, Q.Y., and Wells, J.C., 2008, "Numerical Modelling of Bedform Development; Formation of Sand-Wavelets in Hydrodynamically Smooth Flow over an Erodible Bed," Annual Journal of Hydraulic Engineering, JSCE, **52**, pp. 163-168.

[3]   Yalin. M. S, 1977, Mechanics of Sediment Transport, Pergamon Press.

[4]   Fredsøe, J., and Deigaard R., 1992, Mechanics of Coastal Sediment Transport, World Scientific Pub Co Inc.

[5] Z Liu, 2001, Sediment Transport, Laboratoriet for Hydraulik og Havnebygning, Institut for Vand, Jord og Miljøteknik, Aalborg Universitet.

[6] Sumer B. M., and Bakioglu M., 2006, "On the Formation of Ripples on an Erodible Bed," Journal of Fluid Mechanics, **144**, pp. 177–190.

[7] Keylock C., Hardy R., Parsons D., Ferguson R., Lane S., and Richards K., 2005, "The Theoretical Foundations and Potential for Large-Eddy Simulation (LES) in Fluvial Geomorphic and Sedimentological Research," Earth-Science Reviews, **71**(3-4), pp. 271-304.

[8] Giri S., and Shimizu Y., 2006, "Numerical Computation of Sand Dune Migration with Free Surface Flow," Water Resources Research, **42**(10), p. 10422.

[9] Chang, Yeon S., and Scotti, Alberto, 2003, "Entrainment and Suspension of Sediments into a Turbulent Flow over Ripples," Journal of Turbulence, **4**(1), p. 019.

[10] Mantz P. A., 1992, "Cohesionless Fine-Sediment Bed Forms in Shallow Flows," Journal of Hydraulic Engineering, **118**(5), pp. 743–764.

[11] Coleman S. E., and Melville B. W., 1996, "Initiation of Bed Forms on a Flat Sand Bed," J. Hydr. Engrg., **122**(6), pp. 301-310.

[12] Coleman S. E., Fedele J. J., and Garcia M. H., 2003, "Closed-Conduit Bed-Form Initiation and Development," J. Hydr. Engrg., **129**(12), pp. 956-965.

[13] Langlois V., and Valance A., 2007, "Initiation and Evolution of Current Ripples on a Flat Sand Bed under Turbulent Water Flow," The European Physical Journal E: Soft Matter and Biological Physics, **22**(3), pp. 201–208.

[14] Richards K. J., 1980, "The Formation of Ripples and Dunes on an Erodible Bed," Journal of Fluid Mechanics, **99**(03), pp. 597-618.

[15] Lévêque E., Toschi F., Shao L., and Bertoglio J. P., 2007, "Shear-improved Smagorinsky model for large-eddy simulation of wall-bounded turbulent flows," Journal of Fluid Mechanics, **570**, pp. 491–502.

[16] Fadlun E. A., Verzicco R., Orlandi P., and Mohd-Yusof J., 2000, "Combined Immersed-Boundary Finite-Difference Methods for Three-Dimensional Complex Flow Simulations," J. Comput. Phys., **161**(1), pp. 35-60.

[17] Cheng N., 2002, "Exponential Formula for Bedload Transport," J. Hydr. Engrg., **128**(10), pp. 942-946.

[18] Kovacs , A., and Parker G., 1994, "A New Vectorial Bedload Formulation and its Application to the Time Evolution of Straight River Channels," Journal of Fluid Mechanics, **267**, pp. 153–183.

[19] Kennedy J. F., 1963, "The Mechanics of Dunes and Antidunes in Erodible-Bed Channels," Journal of Fluid Mechanics, **16**, pp. 521–544.

[20] Nakagawa H., and Tsujimoto T., 1980, "Sand Bed Instability due to Bed Load Motion," J. Hydraul. Div, **106**, pp. 2029–2051.

[21] Phillips B. C., and Sutherland A. J., 1989, "Spatial Lag Effects in Bed Load Sediment Transport," Journal of Hydraulic Research JHYRAF, **27**(1).

[22] Bui, Minh Duc, Wenka T., and Rodi W., 2004, "Numerical Modeling of Bed Deformation in Laboratory Channels," J. Hydr. Engrg., **130**(9), pp. 894-904.

[23] Armanini A., and Di Silvio G., 1988, "One-Dimensional Model for the Transport of a Sediment Mixture in Non-Equilibrium Conditions," Journal of Hydraulic Research JHYRAF, **26**(3).

[24] Thuc T., 1991, "Two-Dimensional Morphological Computations Near Hydraulic Structures," Doctoral dissertation, Asian Institute of Technology, Bangkok.

[25] Wu W., Vieira D. A., and Wang S. S., 2004, "One-Dimensional Numerical Model for Non-uniform Sediment Transport under Unsteady Flows in Channel Networks," Journal of Hydraulic Engineering, **130**(9), pp. 914–923.

[26] Geurts B., 2003, Elements of Direct and Large-Eddy Simulation, RT Edwards.

[27] De Angelis V., Lombardi P., and Banerjee S., 1997, "Direct Numerical Simulation of Turbulent Flow over a Wavy Wall," Phys. Fluids, **9**(8), pp. 2429-2442.

[28] Kuru W. C., Leighton D. T., and McCready M. J., 1995, "Formation of Waves on a Horizontal Erodible Bed of Particles," International Journal of Multiphase Flow, **21**(6), pp. 1123–1140.